Editors' Suggestion

Prethermal quantum many-body Kapitza phases of periodically driven spin systems

Alessio Lerose,[1,2] Jamir Marino,[3,*] Andrea Gambassi,[1,2] and Alessandro Silva[1]
[1]*SISSA–International School for Advanced Studies, via Bonomea 265, 34136 Trieste, Italy*
[2]*INFN, Sezione di Trieste, via Bonomea 265, 34136 Trieste, Italy*
[3]*Institut für Theoretische Physik, Universität zu Köln, D-50937 Cologne, Germany;*
Department of Physics and Center for Theory of Quantum Matter, University of Colorado Boulder, Boulder, Colorado 80309, USA;
and Department of Physics, Harvard University, Cambridge Massachusetts 02138, USA

(Received 23 May 2018; revised manuscript received 28 June 2019; published 30 September 2019)

As realized by Kapitza long ago, a rigid pendulum can be stabilized upside down by periodically driving its suspension point with tuned amplitude and frequency. While this dynamical stabilization is feasible in a variety of systems with few degrees of freedom, it is natural to search for generalizations to multiparticle systems. In particular, a fundamental question is whether, by periodically driving a single parameter in a many-body system, one can stabilize an otherwise unstable phase of matter against all possible fluctuations of its microscopic degrees of freedom. In this paper, we show that such stabilization occurs in experimentally realizable quantum many-body systems: A periodic modulation of a transverse magnetic field can make ferromagnetic spin systems with long-range interactions stably trapped around unstable paramagnetic configurations as well as in other unconventional dynamical phases with no equilibrium counterparts. We demonstrate that these quantum Kapitza phases have a long lifetime and can be observed in current experiments with trapped ions.

DOI: 10.1103/PhysRevB.100.104306

I. INTRODUCTION

Periodic drivings are ubiquitous in natural phenomena and particularly in applications ranging from electronics to condensed-matter physics [1–3]. Understanding driven systems is of paramount importance in the context of quantum technologies, since these systems can both realize peculiar phases of matter and help manipulate quantum information [4]. In fact, time-periodic protocols have been theoretically proposed and experimentally realized to engineer a variety of systems, including topological phases [5], time crystals [6,7], and exotic Bose-Einstein condensates [8]. All of them have no equilibrium counterparts, i.e., they do not exist in the absence of driving. For instance, a gas of bosons may condense in a nonuniform, π-quasimomentum state in the presence of a rapidly varying electric field or of a shaken lattice [8]. Similarly, while invariance under time translations cannot be broken at equilibrium, the formation of discrete time crystals under the effect of AC-driving has been theoretically proposed [6] and experimentally observed [7].

In systems with few degrees of freedom, a periodic drive might have spectacular effects, such as the stabilization of a pendulum upside down. A theory of this phenomenon was formulated by P. Kapitza in 1951 [9], and found applications in laboratories (see, e.g., Refs. [10,11]) as well as to the stabilization of otherwise unstable phases (referred to as *Kapitza phases*) in many-body systems whose description, at the mean-field level, can be reduced to a few collective degrees of freedom (see, e.g., Refs. [12–15]). In this paper, we demonstrate that this stabilization may occur over a parametrically large timescale in Floquet prethermal phases of periodically driven quantum magnets affected by many-body fluctuations.

Although the results presented here are general, we focus on experimentally relevant models, i.e., spin chains with long-range ferromagnetic interactions described by the Hamiltonian

$$H = -\sum_{i\neq j}^{N} \frac{J}{|i-j|^{\alpha}} \sigma_i^x \sigma_j^x - B \sum_{i=1}^{N} \sigma_i^z, \tag{1}$$

where σ_i^{μ}s are Pauli matrices, $\alpha, J > 0$ (when $0 \leqslant \alpha < 1$ the scaling $J \propto N^{\alpha-1}$ yields a meaningful thermodynamic limit [16]), and the magnetic field B is periodically varied,

$$B(t) = B_0 + \delta B \cos(\Omega t). \tag{2}$$

These systems accurately model the nonequilibrium dynamics of quantum simulators with trapped ions ($0 < \alpha < 3$) [17,18] or Rydberg atoms ($\alpha = 6$) [19,20]. In Fig. 1, our main findings are illustrated: The nonequilibrium phase diagram of the driven systems features a number of dynamically stabilized phases, which include many-body analogs of the Kapitza pendulum as well as unconventional magnetically ordered phases with no equilibrium counterpart.

II. INFINITE-RANGE SYSTEMS

To gain insight into the physics of this problem, it is worth starting by analyzing the simplest limit $\alpha \to 0$, where mean-field theory becomes exact and ideas analogous to those employed by Kapitza in 1951 can be applied [9]. In fact, in this limit H in Eq. (1) reduces to the Lipkin-Meshkov-Glick model, which is equivalent to a single macroscopic spin [21]

*jamirmarino@fas.harvard.edu

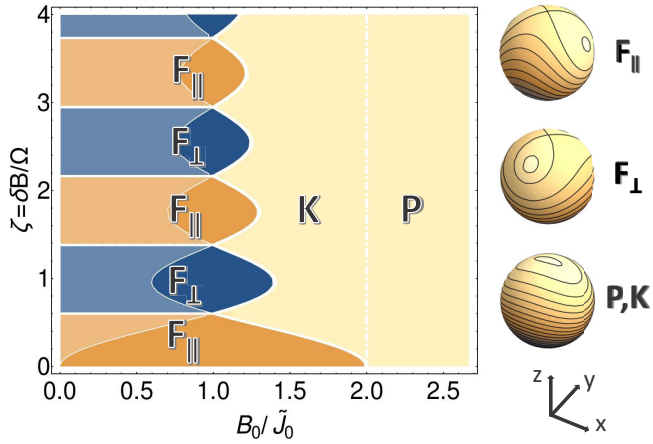

FIG. 1. Left: Fast-driving nonequilibrium phase diagram of the periodically driven long-range Ising model defined by Eqs. (1) and (2). Upon varying the average magnetic field B_0 and the rescaled modulation amplitude $\zeta = \delta B/\Omega$, a dynamical paramagnetic phase P, a dynamically stabilized Kapitza paramagnetic phase K, a conventional dynamical ferromagnetic phase $F_\parallel$, and an unconventional dynamical ferromagnetic phase $F_\perp$ with orthogonal magnetization emerge. The axis $\zeta = 0$ corresponds to the equilibrium phase diagram, where a ferromagnetic $F_\parallel$ and a paramagnetic P phase are present. The diagram shows the exact phase boundaries of the infinite-range system with $\alpha = 0$. (Note that the dashed line separating K and P does not correspond to an actual phase transition.) When $0 < \alpha \leqslant 2$, quantum fluctuations modify these boundaries, leaving, however, their qualitative structure unaltered. Within the shaded region on the left, a second Kapitza phase coexists with $F_{\parallel,\perp}$, but is stable for $\alpha = 0$ only. Right: Schematic phase portraits on the Bloch sphere of the effective high-frequency Hamiltonians governing the evolution of the collective spin of the system, highlighting the various phases. These phases persist up to timescales $\tau \sim \exp(\text{const} \times \Omega/\tilde{J}_0)$ for finite driving frequencies Ω larger than the characteristic energy scale $\tilde{J}_0 = \sum_r^N J/r^\alpha$ of the system, before eventual heating takes place.

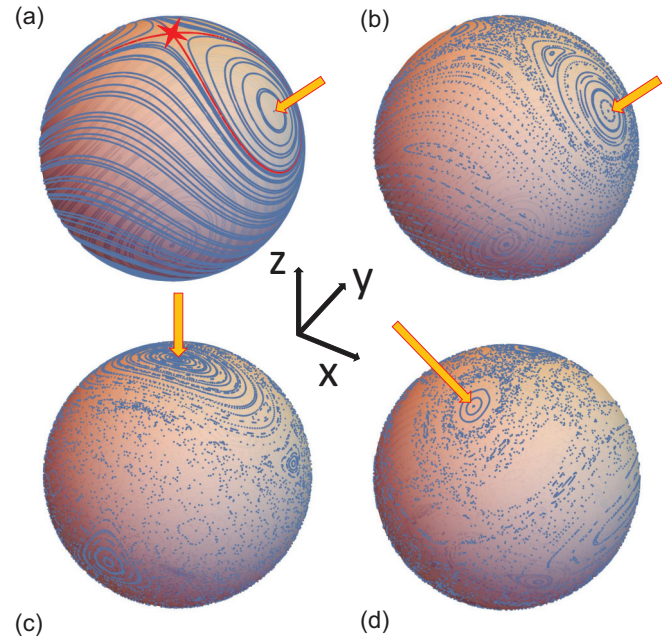

FIG. 2. Dynamics on the Bloch sphere of the infinite-range ($\alpha = 0$) ferromagnet in the thermodynamic limit. (a) Semiclassical phase space trajectories of the static Hamiltonian ($\delta B = 0$) with $B/\tilde{J}_0 = 1.2$. (b)–(d): Stroboscopic trajectories $\{\vec{S}(t_n)\}$, with $t_n = 2\pi n/\Omega$, $n = 0, 1, 2, \ldots$ of the semiclassical collective spin on the Bloch sphere with driving frequency $\Omega/\tilde{J}_0 = 5$ and increasing $\delta B/\tilde{J}_0 = 0.01$ (b), 3.3 (c), and 5 (d), with $B_0/\tilde{J}_0 = 1.2$. Panel (b) shows the presence of a possible ferromagnetic dynamical ordering, corresponding to the evolution occurring within a single ferromagnetic sector $S_x > 0$, with a special synchronized trajectory (appearing as a single point under stroboscopic observations), together with the onset of chaotic behavior around the unstable paramagnetic point [26]. Panel (c) shows the appearance of a dynamically stabilized phase, akin to the well-known stabilization of the inverted driven Kapitza pendulum [9,30]. Panel (d) shows that for larger driving frequencies, an unconventional dynamical ferromagnetic ordering appears, where the direction of the magnetization is orthogonal to the direction x of the actual ferromagnetic interactions. Islands with stable stroboscopic trajectories are indicated by the arrows.

on the Bloch sphere. Indeed, the coupling strength is the same $J = \tilde{J}_0/N$ for all pairs of spins, hence H describes the dynamics of a single collective spin $\vec{S} = \sum_i \vec{\sigma}_i/N$ [22–24]. In the thermodynamic limit $N \to \infty$, the rescaled Hamiltonian H/N becomes equivalent to its classical limit $\mathcal{H}_{\rm cl} = -\tilde{J}_0 S_x^2 - B S_z$. At zero temperature and constant B, this system has a paramagnetic phase for $|B| > 2\tilde{J}_0$, where all the microscopic spins are oriented along the transverse direction z of the field, and a ferromagnetic phase for $|B| < 2\tilde{J}_0$, where the spins acquire a nonvanishing component along the longitudinal direction x [22,23,25].

A. Dynamics

The nonequilibrium evolution of the system in the presence of a time-dependent field $B = B(t)$ is described by the dynamics of the collective spin $\vec{S}(t)$ on the sphere of radius 1 governed by the classical Hamiltonian $\mathcal{H}_{\rm cl}(t)$. When $B = B_0$ is static and supports the ferromagnetic state indicated by the arrow in Fig. 2(a), $\vec{S}(t)$ follows one of the trajectories represented on the Bloch sphere in Fig. 2(a), selected by the initial condition $\vec{S}(0)$ (for definiteness, we will assume $B_0 \geqslant 0$ throughout). Two families of them are characterized by a ferromagneticlike, symmetry-breaking periodic evolution with opposite signs of the nonvanishing time-averaged order parameter $\overline{S_x}$. A trajectory (red) passing through the equilibrium unstable paramagnetic point (red star) separates these two families from the paramagneticlike orbits with $\overline{S_x} = 0$. Turning on the modulation as in Eq. (2), representative samples of discrete stroboscopic trajectories $\{\vec{S}(t_n)\}$, where $t_n = 2\pi n/\Omega$, with $n = 0, 1, 2, \ldots$ of the semiclassical collective spin are reported in Figs. 2(b)–2(d). When the modulation δB is small [see Fig. 2(b)], the equilibrium ferromagnetic states leave room to periodic trajectories of the collective spin within the corresponding ferromagnetic sector *synchronized* with the drive (and hence appearing as a single point under stroboscopic observations). Conversely, initial states in a neighborhood of the unstable paramagnetic point [red star in Fig. 2(a)] display chaotic motion as soon as $\delta B \neq 0$ [25,26]. As δB

increases, this chaotic region invades an increasingly large portion of the sphere [26]. This behavior can be understood on the basis of classical KAM and chaos theory [27,28] and related phenomena have been experimentally observed with Bose-Einstein condensates [29]. Upon further increasing the modulation δB [see Fig. 2(c)], a region in the parameter space emerges where *dynamical stabilization* of the unstable paramagnetic point occurs, thereby opening up a stability region around it. This phenomenon is analogous to the stabilization of the inverted pendulum discovered by Kapitza [9,30]. In addition to this Kapitza-like stabilization, as δB increases with $B_0 \approx \tilde{J}_0$ [see Fig. 2(d)], an unconventional regime appears characterized by dynamical ferromagnetic ordering in the yz plane, orthogonal to the direction x of the actual ferromagnetic interactions.

B. Fast-driving limit

To understand later on the full many-body case ($\alpha \neq 0$), we first analyze the behavior of the system described above in the regime of fast-driving $\Omega \to \infty$ as a function of the rescaled amplitude $\zeta = \delta B/\Omega$. In fact, the effective Floquet Hamiltonian governing the stroboscopic evolution [31] can be determined nonperturbatively, by switching to a convenient oscillating reference frame [2] (see Appendix A). The effect of the driving then amounts to redistributing the ferromagnetic coupling strength along the directions x and y, thereby turning the Ising model into an XY model, with

$$\mathcal{H}_{\rm eff} = -\tilde{J}_0\left(\frac{1+\gamma(\zeta)}{2}S_x^2 + \frac{1-\gamma(\zeta)}{2}S_y^2\right) - B_0\, S_z, \qquad (3)$$

and anisotropy parameter $\gamma(\zeta) = \mathcal{J}_0(4\zeta)$, where $\mathcal{J}_0$ is the Bessel function of the first kind.

As ζ increases from zero, the effective ferromagnetic interaction along x weakens, which makes it possible to dynamically stabilize the paramagnetic configuration. The exact boundary $B_0 = B_{\rm cr}(\zeta) \equiv \tilde{J}_0(1 + |\mathcal{J}_0(4\zeta)|)$ of the Kapitza phase K is reported in Fig. 1. Note that this region is continuously connected with the paramagnetic one P in the phase diagram, see Fig. 1, similarly to the region of dynamical stabilization of the Kapitza pendulum, which is continuously connected with the parameter region corresponding to a reversed direction of gravity, in which stability is trivial [30]. As ζ increases even further, due to the oscillations of $\mathcal{J}_0$ around zero, intervals with a negative anisotropy γ appear, favoring ferromagnetic ordering along the y direction. This explains the occurrence of the unconventional dynamical phases with ferromagnetic ordering in the yz plane, orthogonal to the direction x of the actual ferromagnetic interaction, which builds up whenever $\gamma < 0$, $B_0 < \tilde{J}_0(1-\gamma)$, i.e., within the regions denoted by $F_\perp$ in Fig. 1. A second Kapitza phase coexists with $F_{\parallel,\perp}$ for $B_0 < \tilde{J}_0(1 - |\mathcal{J}_0(4\zeta)|)$, as discussed in Appendix D.

The numerical results reported in Fig. 2 show that these nonequilibrium phases persist even at smaller driving frequencies, comparable to the characteristic energy scale $\tilde{J}_0$ of the system. Indeed, as discussed in Appendix A, when the driving frequency Ω is large but finite, the effective Floquet Hamiltonian Eq. (3) receives perturbative corrections in an expansion in inverse powers of Ω. The first term beyond Eq. (3) is reported in Appendix B [cf. Eq. (B1)] and it causes small quantitative modifications of the boundaries in Fig. 1. Furthermore, this dynamical stabilization is robust to finite-size effects, as demonstrated in Sec. III C below.

III. VARIABLE-RANGE INTERACTIONS

The behavior of infinite-range systems can essentially be understood in terms of one-body physics. However, when interactions have a nontrivial spatial dependence, fluctuations at all length scales are activated. The possibility to stabilize many-body dynamical phases by modulating in time a global external field represents a major conceptual and practical challenge. To address this problem, we study below the spin system Eq. (1) with $\alpha \neq 0$ and we will show how the dynamical phases reported above can be stabilized also for $0 < \alpha \leqslant 2$, where quantum fluctuations around the semiclassical evolution are not suppressed, with the exception of the coexistence region. Their effect is reduced by decreasing the parameter α, which continuously connects these models with their infinite-range semiclassical limit.

When $\alpha \neq 0$, both the total spin $\vec{S}$, corresponding to the $k = 0$ Fourier mode of $\vec{\sigma}_i$, and all the $k \neq 0$ quasiparticle (*spin wave*) excitations are affected by interactions [32,33]. To account for the coupled dynamics of the collective spin and of the spin-wave excitations around the time-dependent direction of $\vec{S}(t)$, we employ the *time-dependent spin-wave theory* developed in Ref. [32], see also Appendix C for a concise overview. In the presence of $k \neq 0$ modes, representing all microscopic fluctuations, the system may be thought of as a macroscopic semiclassical collective degree of freedom, i.e., the total spin $\vec{S}(t)$, which "drags" an extensive set of quantum oscillators $(\tilde{q}_k, \tilde{p}_k)$'s, i.e., of microscopic degrees of freedom corresponding to the bosonic spin wave excitations with quasimomentum $k \neq 0$ [32,33]. Indeed, the time-dependent spin-wave theory maps spin fluctuations into such bosonic excitations and the Hamiltonian $H(t)$ is then written in terms of the collective spin variables $\vec{S}/|\vec{S}| = (\sin\theta\cos\phi, \sin\theta\sin\phi, \cos\theta)$ and of the spin wave operators $\tilde{q}_k$'s, $\tilde{p}_k$'s. Truncation to quadratic order in the quantum fluctuations yields

$$\begin{aligned} H(t) = &-NB(t)(1-\epsilon)\cos\theta - N\tilde{J}_0[(1-\epsilon)\sin\theta\cos\phi]^2 \\ &- 4\sum_{k\neq 0}\tilde{J}_k\Bigg(\cos^2\theta\cos^2\phi\,\frac{\tilde{q}_k\tilde{q}_{-k}}{2} + \sin^2\phi\,\frac{\tilde{p}_k\tilde{p}_{-k}}{2} \\ &- \cos\theta\cos\phi\sin\phi\,\frac{\tilde{q}_k\tilde{p}_{-k} + \tilde{p}_k\tilde{q}_{-k}}{2}\Bigg), \end{aligned} \qquad (4)$$

where $\tilde{J}_k$ is the Fourier transform of the interaction J/r^α (the scaling of J as $N \to \infty$, see below Eq. (1), guarantees that $\tilde{J}_0$ is finite in the thermodynamic limit) and $\epsilon = \sum_k(\tilde{q}_k\tilde{q}_{-k} + \tilde{p}_k\tilde{p}_{-k} - 1)/N$ is the relative depletion of the total spin length from its maximal value, i.e., $|\vec{S}| = 1 - \epsilon$. The last term in Eq. (4) accounts for the interaction between the collective semiclassical spin $\vec{S}$ and the quantum spin-wave excitations.

A. Dynamically stabilized many-body phases

A many-body Kapitza phase consists of a simultaneous dynamical stabilization of the whole spectrum of quantum

excitations around an unstable paramagnetic configuration. Intuition on this phenomenon can be obtained at the level of linear stability by expanding $H(t)$ to quadratic order in the quantum fluctuations, as in Eq. (4), around the point $\theta = 0$:

$$H(t) = E(t) + 2\sum_k \left[(B(t) - 2\tilde{J}_k)\frac{\tilde{q}_k \tilde{q}_{-k}}{2} + B(t)\frac{\tilde{p}_k \tilde{p}_{-k}}{2} \right], \tag{5}$$

where $E(t) = -2NB(t)$ and $k = 2\pi n/N$ with $n = 0, 1, \ldots, N-1$ (assuming periodic boundary conditions for simplicity). In the absence of modulation in the ferromagnetic phase [i.e., $B(t) = B_0 < 2\tilde{J}_0$], an extended interval near $k = 0$ in the spin-wave band corresponds to unstable modes, as their corresponding frequency $\omega_k = 2[B_0(B_0 - 2\tilde{J}_k)]^{1/2}$ becomes imaginary for $\tilde{J}_k > B_0/2$. However, upon introducing the modulation $B(t)$ as before, the effective dispersion relation is modified and, for a suitable choice of the driving parameters, ω_k may become real for all values of k. The occurrence of this nontrivial stabilization of an otherwise unstable phase of matter against all possible fluctuations of its degrees of freedom is illustrated in Fig. 3 and it represents an actual generalization of the Kapitza pendulum to a genuine many-body system.

To understand how all the degrees of freedom can get dynamically and simultaneously stabilized by driving a single global field $B(t)$, we concentrate first on the fast-driving limit $\Omega \to \infty$ as a function of the rescaled driving amplitude ζ, which can be studied analytically also for $\alpha \neq 0$. Here, the effective Floquet Hamiltonian governing the stroboscopic time-evolution is the long-range XY spin chain,

$$H_{\rm eff} = -\sum_{i\neq j}^{N} \frac{J}{|i-j|^\alpha}\left(\frac{1+\gamma(\zeta)}{2}\sigma_i^x\sigma_j^x + \frac{1-\gamma(\zeta)}{2}\sigma_i^y\sigma_j^y\right) - B_0\sum_i^N \sigma_i^z, \tag{6}$$

where the parameter $\gamma(\zeta)$ is the same as in Eq. (3) and is independent of the particular dependence of the interactions on the distance (see Appendix A).

The stability analysis of the paramagnetic configurations is carried out by expanding $H_{\rm eff}$ at the quadratic order in the spin-wave operators around the field direction z and hence by determining the range of parameter values within which the dispersion relation is real. It turns out that a simultaneous dynamical stabilization of the whole spectrum of spin-wave excitations, such as that illustrated in Fig. 3, is possible within the region denoted by K in Fig. 1, and, upon increasing α, the quantum fluctuations solely modify its phase boundary. Within the shaded region in Fig. 1, instead, the second Kapitza phase turns out to be unstable to many-body fluctuations at finite wavelength: Although the driving stabilizes the collective mode with $k = 0$, an extended interval in the Brillouin zone with $k \neq 0$ appears, which is characterized by imaginary frequencies (see Appendix D for further details). To the lowest order in $\tilde{J}_{k\neq 0}$, the shift $\Delta B_{\rm cr}(\zeta)$ of the left boundary

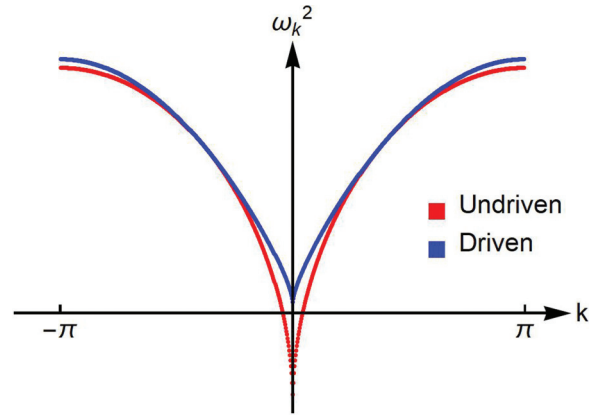

FIG. 3. Stabilization of the *many-body* Kapitza phases. In the presence of a suitable periodic driving, the otherwise unstable spectrum of quantum excitations around the paramagnetic configuration gets simultaneously dynamically stabilized for all values of k. Here $\alpha = 1.5$, $N = 400$, and $B_0/\tilde{J}_0 = 1.35$: In the absence of the driving $\delta B = 0$, the system is in the ferromagnetic phase. The red points represent the (squared) frequency spectrum $\omega_k^2 = 4B_0(B_0 - 2\tilde{J}_k)$ of the spin-wave excitations, labeled by their wave vector k, with an extended interval of *unstable* long-wavelength modes (i.e., $\omega_k^2 < 0$ for k near 0). As the driving is turned on with a strength in a suitable range of values, not only the collective spin mode with $k = 0$ discussed in Sec. II, but also the whole set of modes with $k \neq 0$ become *stable* (i.e., $\omega_k^2 > 0$ for all k). The blue points show the exact effective dispersion relation $\omega_k^2 = 4(B_0 - \tilde{J}_k)^2$ in the presence of a high-frequency driving $\Omega \to \infty$ with $\zeta = \delta B/\Omega = 0.6014$ (corresponding to $\gamma = 0$ in the effective Hamiltonian, see the text). When $\tilde{J}_0 \ll \Omega < \infty$, this effective dispersion relation receives perturbative corrections in inverse powers of Ω, thus no qualitative changes occur as long as the system is in the prethermal regime (see Sec. III B and references therein). As discussed in the text, upon decreasing α below 1, the Fourier transform $\tilde{J}_k$ of the ferromagnetic couplings approaches zero for all $k \neq 0$ in the thermodynamic limit, thus reducing this many-body problem to the single-body dynamical stabilization of the collective spin discussed in Sec. II.

$B_0 = B_{\rm cr}(\zeta)$ of region K is given by

$$\Delta B_{\rm cr}(\zeta) = -\tilde{J}_0|\gamma(\zeta)|\left[\int_{-\pi}^{\pi}\frac{dk}{\pi}\left(\frac{\tilde{J}_k}{\tilde{J}_0}\right)^2\right]\frac{1+\frac{3}{2}|\gamma(\zeta)|}{1+|\gamma(\zeta)|}, \tag{7}$$

as derived in Appendix E. Due to the rescaling of long-range interactions in the thermodynamic limit [see below Eq. (1)], one has $\tilde{J}_{k\neq 0} \to 0$ when $0 < \alpha \leqslant 1$ (i.e., as $N \to \infty$ fluctuations are suppressed and the system becomes equivalent to its infinite-range limit), whereas $\tilde{J}_{k\neq 0}$ approaches a finite value when $1 < \alpha \leqslant 2$, with a cusp behavior $\tilde{J}_{k\neq 0} \sim \tilde{J}_0(1 - c|k|^{\alpha-1})$ for small wave numbers k. Accordingly, the modification of the phase boundary in Fig. 1 due to quantum fluctuations is vanishingly small in the thermodynamic limit when $0 < \alpha \leqslant 1$ and is finite as $\alpha > 1$, the smallness parameter being $\alpha - 1$. The resulting modified nonequilibrium phase diagram is presented in Fig. 4.

This proves the *existence* of many-body nonequilibrium Kapitza phases for sufficiently fast driving (and in the regime of prethermal slow heating, see Sec. III B below), under the sole condition that the effect of fluctuations is not so strong as to modify the bulk structure of the equilibrium phases of the

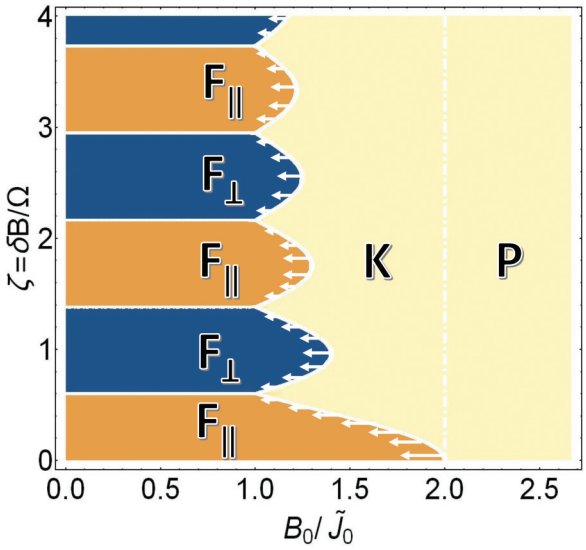

FIG. 4. Fast-driving nonequilibrium phase diagram of the periodically driven long-range Ising model defined by Eqs. (1) and (2), for $\alpha > 0$. Compared to Fig. 1, the shaded region of coexistence of phase K with $F_{\parallel,\perp}$ has disappeared, and the left boundary of region K moves leftward upon increasing α, as determined by Eq. (7) and indicated by the white arrows. This displacement is vanishingly small in the thermodynamic limit for $0 < \alpha \leqslant 1$, due to the rescaling of long-range interactions as $N \to \infty$ [see below Eq. (1)], whereas it is finite for $\alpha > 1$. The amount indicated by the arrows corresponds to Eq. (7) with $\alpha = 1.5$ (it is magnified by a factor of 2 for ease of visualization).

effective Hamiltonian $H_{\rm eff}$, which is known to be generally the case for long-range interactions with exponent $\alpha \leqslant 2$, as well as for higher-dimensional systems with short-range interactions [16,34].

More generally, the stability of the various many-body nonequilibrium phases can be determined by studying the local extrema of the mean-field energy landscape of $H_{\rm eff}$ and the corresponding spectra of excitations. In particular, driving amplitudes ζ corresponding to negative anisotropy parameters $\gamma(\zeta) < 0$ allow the appearance of dynamically stabilized unconventional ferromagnetic phases with orthogonal ferromagnetic ordering in the yz plane whenever $B_0 < \tilde{J}_0(1-\gamma) + \Delta B_{\rm cr}$ [cf. Eq. (7)], which have no equilibrium counterpart in the Ising model. Such phases arise under the same conditions as the Kapitza phases discussed above.

B. Prethermalization and heating

We address here the footprint of the fast-driving nonequilibrium phase diagram on the finite-frequency dynamics, upon reducing Ω down to a scale comparable with the microscopic energy scale $\tilde{J}_0$ of the system. In this case, one should expect the system to eventually absorb an ever-increasing amount of energy from the drive [35,36]. To investigate this point, we initialize the system in various fully polarized states parameterized by angles (θ_0, ϕ_0) on the Bloch sphere and study the nonequilibrium evolution for various values of $\alpha > 0$ and driving parameters $B_0, \delta B, \Omega$ by numerically integrating the dynamical equations of the time-dependent spin wave theory, where the heating rate can be monitored, e.g., through the depletion of the collective spin magnitude from its maximal value (see Appendix C). The results are illustrated in Fig. 5.

Whenever the system is initialized in a nonchaotic dynamical regime, P, K or $F_{\parallel,\perp}$, and the frequency Ω is off-resonant with the spin-wave band, i.e., $\Omega \gg 4\tilde{J}_0$, as shown in Fig. 5(a), 5(c) and 5(d), the evolution presents a long time interval during which the absorption of energy from the drive, as well as the amount of spin-wave excitations, is bounded. On the other hand, whenever the system is in a chaotic dynamical regime as in Fig. 5(b), irrespective of the value of Ω and of α, the amount of generated spin-wave excitations and the energy increase at a finite rate. Such a behavior corresponds to *heating*, which has been extensively proven to be the generic response of a many-body system to an external periodic driving [35–37], in the absence of dissipative mechanisms [38]. In the nonchaotic dynamical regimes $F_{\parallel,\perp}$ of Figs. 5(a) and 5(d), the synchronized trajectories of the collective spin $\vec{S}(t)$ act as an "internal" periodic driving at frequency Ω on the quantum oscillators $(\tilde{q}_k, \tilde{p}_k)$'s through the last interaction terms in the spin-wave Hamiltonian Eq. (4). As long as Ω is off-resonant (see above), the spin waves behave like a periodically driven system of quasifree particles, which relaxes to a periodic quasistationary state described by a stroboscopic generalized Gibbs ensemble [39,40]. The presence of nonlinear spin-wave interactions cause the latter *prethermal* stage [37,41–44] to be ultimately followed by slow heating, after a parametrically long time τ which scales as $\tau \sim \exp(\text{const} \times \Omega/\tilde{J}_0)$ [36]. On the contrary, the occurrence of chaotic motion of the collective spin $\vec{S}(t)$ translates, as in Fig. 5(b), into an irregular, noisy "internal" driving of the spin waves through the last terms in Eq. (4), possessing a broad frequency spectrum, whereby the unavoidable resonances with the spin waves band together with the local instability trigger the process of internal dissipation and hence a much faster heating.

C. Quantum simulations with trapped ions

We finally address the robustness of the dynamically stabilized nonequilibrium phases to finite-size effects as well as their observability in the setup of quantum simulations with trapped ions. In particular, we computed the nonequilibrium evolution of small driven systems of $N = 16$ spins by numerically integrating the time-dependent many-body Schrödinger equation, and demonstrate the occurrence of quantum many-body Kapitza phases for the long-range interacting chains in Eq. (1) as well as with the space-dependent spin-spin couplings J_{ij} which characterize a chain of trapped ions experimentally investigated in Ref. [17], roughly corresponding to model Eq. (1) with $\alpha \approx 1$.

In Fig. 6, we report an illustration of the stabilization of the *ordered* phase $F_\perp$, which is of greater experimental relevance as it presents a type of magnetic ordering that is absent in the equilibrium phase diagram. To probe its occurrence, the driving parameters in Eq. (2) are chosen well inside the region $F_\perp$ of the nonequilibrium phase diagram in Fig. 4, and the system is initialized in a fully polarized state along the y direction. In the top panel, the stroboscopic time evolution of the orthogonal magnetization $\langle S_y(nT)\rangle$, with $T = 2\pi/\Omega$ and $n = 0, 1, 2, \ldots,$ is shown for the

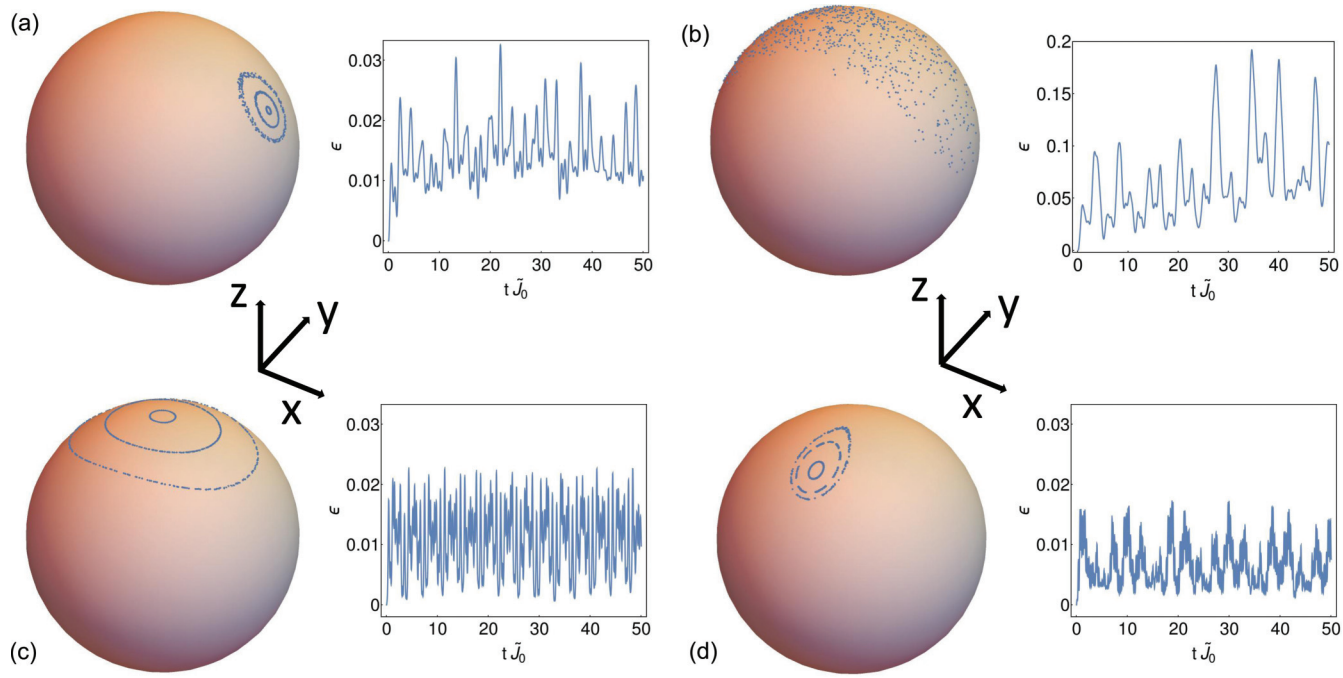

FIG. 5. Persistence of the dynamically stabilized phases at finite driving frequency. Left in each panel: Stroboscopic time evolution of the total spin (projected on the unit sphere) of the long-range Ising chains in Eq. (1) with $\alpha \neq 0$, subject to the modulated magnetic field in Eq. (2). The dynamics is obtained by numerically integrating the system of coupled evolution equations for the total spin and the spin waves provided by the time-dependent spin-wave theory, see Eq. (4) and Appendix C. In all simulations, the static field is $B_0/\tilde{J}_0 = 1.2$, as in Fig. 2, the driving frequency is $\Omega/\tilde{J}_0 = 8$, the system size is $N = 100$, and the system is initialized in spin-coherent (fully polarized) states in the xz [panels (a)–(c)] and yz [panel (d)] planes. Right in each panel: Relative departure $\epsilon(t)$ of the total spin from its maximal length $N/2$ [i.e., $|\vec{S}(t)| = 1 - \epsilon(t)$], due to the generation of quantum spin wave excitations, corresponding to the largest trajectory in each panel. Notice $\epsilon(t = 0) = 0$ with our choice of fully polarized initial states. In particular: (a) Dynamical ferromagnetic phase, with $\alpha = 1$ and $\delta B/\tilde{J}_0 = 0.05$. (b) Fast heating in the chaotic dynamical regime, with $\alpha = 0.8$, $\delta B/\tilde{J}_0 = 0.2$. (c) Dynamically stabilized Kapitza phase, with $\alpha = 1$, $\delta B/\tilde{J}_0 = 5.33$. (d) Unconventional, dynamically stabilized ferromagnetic phase with magnetization in the yz plane orthogonal to the direction x of the actual ferromagnetic interactions, with $\alpha = 1$, $\delta B/\tilde{J}_0 = 8$. Panels (a), (c), and (d) demonstrate that the dynamical phases $F_{\|}$, K, $F_{\perp}$ (see Fig. 1), respectively, continue to exist at finite driving frequency. The amount of excitations generated remains small and the total energy remains bounded across many cycles, qualifying these phases as being *prethermal*. In panel (b), instead, the broad frequency spectrum of the chaotic semiclassical motion gives rise to resonant generation of excitations, witnessed by the growth of $\epsilon(t)$ (notice the different vertical scale in the plot), and absorption of energy from the drive (*heating*). The heating rate in this case increases upon increasing α.

simulated trapped-ion system subject to the drive (magenta) as well as in the limit of vanishing driving strength (blue). In both cases, the shaded region around the symbols indicates the instantaneous quantum uncertainty of the magnetization $\Delta S_y(t) \equiv \sqrt{\langle S_y^2(nT)\rangle - \langle S_y(nT)\rangle^2}$. As the plot clearly shows, in agreement with the theory developed in this paper, the drive stabilizes a magnetic ordering that is not possible in static conditions. We emphasize that the preparation of tilted fully polarized states, the implementation of the considered driving protocols and the measurements of the tilted magnetization can be achieved with standard experimental techniques, which make it possible to actually observe this phenomenon with trapped ions.

To disentangle the finite-frequency and finite-size effects from the effects of having experimentally realistic interactions, we report in the bottom panel of Fig. 6 the outcome of analogous simulations in which the trapped-ion couplings have been replaced by uniform collective interactions $J_{ij} \equiv \tilde{J}_0/(N-1)$ with the same average strength. The qualitative appearance of the two plots is similar, in agreement with our theory. However, we observe that the strong many-body quantum fluctuations affecting data in the top panel have a visible effect in the transient relaxation dynamics: In fact, while the *single-body* collective spin oscillations in the bottom panel become increasingly long-lived in larger systems as the classical limit is approached, the *many-body* spatially decaying interactions in the top panel cause damping and, correspondingly, are expected to lead to a Gibbs-type Floquet prethermal state in terms of the approximate high-frequency Floquet Hamiltonian given by Eq. (6) with the couplings $J/|i-j|^{\alpha}$ replaced by the experimental ones J_{ij} [36].

IV. CONCLUSIONS AND PERSPECTIVES

Dynamical stabilization is a well-understood mechanism since the original work of P. Kapitza in 1951 [9] on the driven classical pendulum and has found several experimental applications, e.g., in particle synchrotrons [10] and in Paul traps [11]. More recently, it has been applied to quantum many-body physics out of equilibrium, for instance, to stabilize Bose-Einstein condensate clouds in two and three spatial dimensions [12], to prevent spin mixing in spinor condensates

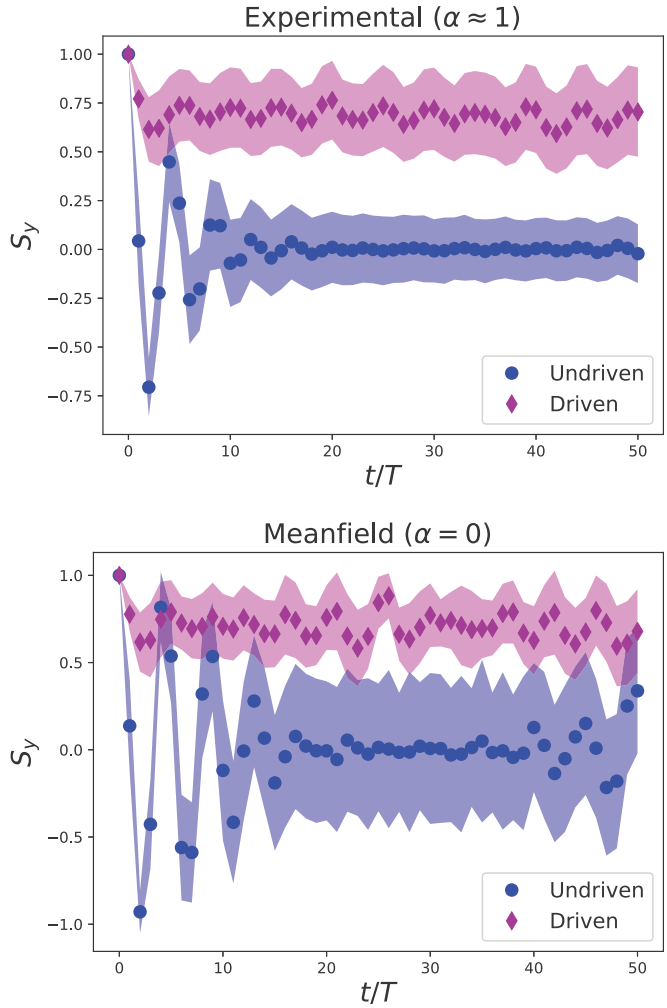

FIG. 6. Illustration of the dynamical stabilization of the unconventional ferromagnetic phase $F_\perp$ in a realistic trapped-ion setup (top panel) and in the corresponding infinite-range system (bottom panel). The orthogonal magnetization $\langle S_y(t)\rangle \pm \Delta S_y(t)$ (see the text) is plotted at stroboscopic times $t = nT$, with $T = 2\pi/\Omega$ and $n = 0, 1, 2, \ldots$, for undriven and driven systems of $N = 16$ spins with the actual space-dependent couplings J_{ij} which characterize a chain of trapped ions experimentally studied in Ref. [17], roughly described by Eq. (1) with $\alpha \approx 1$ and Eq. (2) (top panel). The system is initialized in a fully polarized state in the y direction, and the driving parameters are $B_0/\tilde{J}_0 = 0.5$, $\zeta = 1$, and $\Omega/\tilde{J}_0 = 8$, corresponding to a point well inside a region $F_\perp$ in Fig. 4. For comparison, the corresponding simulation with J_{ij} replaced by all-to-all uniform interactions of equal average strength is shown in the bottom panel. Ferromagnetic ordering in the yz plane is dynamically stabilized by the drive, and is found to be robust to finite driving frequency, finite-size effects and "imperfections" in the long-range couplings, realizing a pre-thermal quantum many-body Kapitza phase observable with trapped-ion quantum simulators.

[13,14], and to stabilize π-modes in driven bosonic Josephson junctions [15]. In all these cases, however, the dynamical stabilization by periodic driving involves a *single* collective mode of the system. The driven infinite-range model which we preliminarily study in Sec. II represents an instance of the same class.

On the other hand, the present paper demonstrates that this dynamical stabilization can occur in the presence of a rather general class of multiparticle interactions, for which the many-body problem cannot be reduced to that of a single collective degree of freedom. In this respect, the mechanism investigated here is a bona-fide realization of the many-body Kapitza pendulum. Moreover, we have shown that *ordered* ferromagnetic phases can also be stabilized via periodic driving, in a way that has no counterpart in equilibrium.

We focused here on the physics of long-range interacting spin chains because of their relevance for current experiments with ion traps [17,18], which can be prepared in fully polarized initial states and whose time evolution can be modeled by Hamiltonians of the form (1). The phenomena that we report are actually even more stable in higher-dimensional systems [20,45] and/or with higher spins [46], where fluctuations are less effective. In this respect, we emphasize that the dynamically stabilized nonequilibrium phases studied in this paper can be observed even in relatively small systems with size $N \gtrsim 16$, accessible to exact numerical simulations and well within the reach of state-of-the-art experiments, as demonstrated in Fig. 6.

We expect that our analysis can be generalized to other important phase transitions involving more complex symmetries, such as in the case of superconductors, providing access to a number of nonequilibrium phases of matter. In addition, our approach can be extended to account for the effects of disorder and of external environments, further corroborating the robustness of our findings.

ACKNOWLEDGMENTS

We thank M. Eckstein, G. Pagano, and A. Polkovnikov for interesting discussions. We thank the authors of Ref. [17] for kindly providing us with the data characterizing the interactions in their experimental setup. J.M. is supported by the European Union's Horizon 2020 research and innovation program under the Marie Sklodowska-Curie Grant Agreement No. 745608 (QUAKE4PRELIMAT).

APPENDIX A: EFFECTIVE (FLOQUET) HAMILTONIAN

Whenever the time-dependent Hamiltonian of a system has a period T, i.e., $H(t+T) = H(t)$, the resulting time-evolution operator $U(t_2, t_1)$ satisfies

$$U(t_0 + nT, t_0) = [U(t_0 + T, t_0)]^n \tag{A1}$$

for any integer n. Accordingly, it is convenient to define an effective static Hamiltonian $H_{\rm eff}$ [2,31],

$$U(t_0 + T, t_0) = \mathcal{T} e^{-i\int_{t_0}^{t_0+T} d\tau\, H(\tau)} \equiv e^{-iTH_{\rm eff}}, \tag{A2}$$

usually referred to as the *Floquet Hamiltonian*. Its spectrum is defined up to integer multiples of the frequency $2\pi/T$ and it is independent of the choice of the reference time t_0. The state of the system at stroboscopic times $t_n = t_0 + nT$ is therefore entirely and unambiguously determined by the Floquet Hamiltonian $H_{\rm eff}$. A series expansion of $H_{\rm eff}$ in powers of the period T, known as the *Magnus expansion*, can be

written as

$$H_{\rm eff} = \sum_{n=0}^{\infty} H_{\rm eff}^{(n)}, \tag{A3}$$

with $H_{\rm eff}^{(n)}$ proportional to T^n. Explicitly, the first terms read

$$H_{\rm eff}^{(0)} = \int_{t_0}^{t_0+T} \frac{d\tau_1}{T} H(\tau_1), \tag{A4}$$

$$H_{\rm eff}^{(1)} = \frac{T}{2} \int_{t_0}^{t_0+T} \frac{d\tau_1}{T} \int_{t_0}^{t_0+\tau_1} \frac{d\tau_2}{T} [H(\tau_1), H(\tau_2)], \tag{A5}$$

with the higher-order terms involving an increasing number of nested commutators of H at different times. This expansion is convergent when T is smaller than the inverse maximal extension of the spectrum of $H(t)$ [31].

We consider in the following the general class of systems defined in Eq. (1), which encompasses the long- and infinite-range Ising chains subject to the effect of the periodic driving in Eq. (2). In the simplest high-frequency limit $\Omega \to \infty$, the effective evolution is governed by the time-averaged Hamiltonian [cf. Eq. (A4)], since the system has no time to react to variations of the external parameters much faster than its characteristic dynamical timescales. Nevertheless, if the modulation amplitude δB is simultaneously increased with fixed $\zeta \equiv \delta B/\Omega$, the effective dynamics becomes qualitatively different from the former. Such qualitative changes involve a resummation of the high-frequency expansion in Eq. (A3) of the Floquet Hamiltonian [2]. In some cases, an analytic solution in closed form can be obtained by performing a convenient time-periodic change of coordinates [2]. Indeed, by moving into the oscillating frame

$$\begin{pmatrix} \sigma_i^x \\ \sigma_i^y \\ \sigma_i^z \end{pmatrix} = \begin{pmatrix} \cos(2\zeta \sin(\Omega t))\sigma_i'^x + \sin(2\zeta \sin(\Omega t))\sigma_i'^y \\ -\sin(2\zeta \sin(\Omega t))\sigma_i'^x + \cos(2\zeta \sin(\Omega t))\sigma_i'^y \\ \sigma_i'^z \end{pmatrix}, \tag{A6}$$

the time-periodicity of the external magnetic field is eliminated, and the proper equations of motion for $\vec{\sigma}'$ are generated by $\widetilde{H}(t)$, the static part of the Hamiltonian alone, which takes the same form as Eq. (1) with $\sigma_i^x \sigma_j^x$ replaced by

$$\begin{aligned} &\cos^2(2\zeta \sin(\Omega t))\sigma_i'^x \sigma_j'^x + \sin^2(2\zeta \sin(\Omega t))\sigma_i'^y \sigma_j'^y \\ &+ \cos(2\zeta \sin(\Omega t)) \sin(2\zeta \sin(\Omega t))\left(\sigma_i'^x \sigma_j'^y + \sigma_i'^y \sigma_j'^x\right). \end{aligned} \tag{A7}$$

Crucially, the modulation δB now intervenes only via the finite combination ζ. A standard high-frequency expansion for the new time-periodic Hamiltonian $\widetilde{H}(t)$ will then reproduce the correct high-frequency effective Hamiltonian $H_{\rm eff}$. To lowest order, time-averaging yields the XY model of Eq. (6) with an engineered anisotropy parameter $\gamma = \gamma(\zeta) = \mathcal{J}_0(4\zeta)$, where $\mathcal{J}_0$ is the standard Bessel function of the first kind.

APPENDIX B: FINITE-FREQUENCY CORRECTIONS

We discuss here the correction of order Ω^{-1} to the effective Hamiltonian Eq. (3) within the Magnus expansion in the oscillating frame (see Appendix A). By using Eq. (A5), a straightforward calculation yields

$$\begin{aligned} \mathcal{H}_{\rm eff}^{(1)} = \frac{8\pi \tilde{J}_0^2}{\Omega} \Big[&\kappa_{x^2,y^2}(\zeta)\, S_x S_y S_z - \kappa_{xy,x^2}(\zeta)\, S_x^2 S_z \\ &+ \kappa_{xy,y^2}(\zeta)\, S_y^2 S_z + \frac{B_0}{2\tilde{J}_0} \kappa_{z,xy}(\zeta) \left(S_y^2 - S_x^2\right) \Big], \end{aligned} \tag{B1}$$

in terms of the dimensionless coefficients κ

$$\begin{aligned} \kappa_{x^2,y^2}(\zeta) &= \int_0^{2\pi} \frac{d\xi}{2\pi} (\dot{A}B - \dot{B}A), \\ \kappa_{xy,x^2}(\zeta) &= \int_0^{2\pi} \frac{d\xi}{2\pi} (\dot{C}A - \dot{A}C), \\ \kappa_{xy,y^2}(\zeta) &= \int_0^{2\pi} \frac{d\xi}{2\pi} (\dot{C}B - \dot{B}C), \\ \kappa_{z,xy}(\zeta) &= \int_0^{2\pi} \frac{d\xi}{2\pi} C, \end{aligned} \tag{B2}$$

where the dots stand for derivatives with respect to the argument ξ, and

$$\begin{aligned} A(\xi) &\equiv \int_0^{\xi} \frac{d\eta}{2\pi} \cos^2(2\zeta \sin\eta), \\ B(\xi) &\equiv \int_0^{\xi} \frac{d\eta}{2\pi} \sin^2(2\zeta \sin\eta) = \frac{\xi}{2\pi} - A(\xi), \\ C(\xi) &\equiv \int_0^{\xi} \frac{d\eta}{2\pi} \cos(2\zeta \sin\eta) \sin(2\zeta \sin\eta). \end{aligned} \tag{B3}$$

The classical Hamiltonian $\mathcal{H}_{\rm eff}^{(0)} + \mathcal{H}_{\rm eff}^{(1)}$, with $\mathcal{H}_{\rm eff}^{(0)}$ given by Eq. (3) and $\mathcal{H}_{\rm eff}^{(1)}$ by Eq. (B1), defines phase space trajectories on the Bloch sphere which better approximate the stroboscopic evolution of the collective spin at finite driving frequency Ω compared to the high-frequency limit Eq. (3). In particular, it is possible to determine the shift of the boundaries in Fig. 1 to order Ω^{-1}. We note that although the Magnus expansion is divergent [2], its truncations provide an increasingly accurate approximation of the regular orbits (KAM tori) in phase space, and hence of the dynamically stabilized phases.

APPENDIX C: TIME-DEPENDENT SPIN WAVE THEORY

We briefly outline here this method, developed in Ref. [32], which provides a natural and viable approach to investigate the equilibrium phases and the non-equilibrium evolution of a wide class of spin models.

A time-dependent reference frame $\mathcal{R} = (\hat{X}, \hat{Y}, \hat{Z})$ is introduced, with its $\hat{Z}$ axis following the collective motion of $\vec{S}(t)$. The change of frame is implemented by a time-dependent global rotation operator parameterized by the spherical angles $\theta(t)$ and $\phi(t)$, whose evolution will be self-consistently determined in such a way that $S_X(t) \equiv S_Y(t) \equiv 0$. For $\alpha = 0$, when H is a function of the total spin $\vec{S}$ only, this requirement translates into a closed pair of ordinary differential equations for the two angles, as in Fig. 2. For $\alpha > 0$, the dependence of the interactions on the distance renders H a function not only of the total spin, i.e., the $k = 0$ Fourier mode of the spins, but also of all the k modes of the spins, which now contribute

to the dynamics. To systematically take into account these fluctuations, the $\vec{\sigma}_i$ spins' deviations from the instantaneous direction of the $\hat{Z}$ axis are mapped to bosonic variables q_i, p_i via Holstein–Primakoff transformations. The nonequilibrium dynamics of the system governed by the Hamiltonian Eq. (1) with $\alpha \neq 0$ involves quantum corrections to the classical evolution of the total spin $\vec{S}(t)$, which are expressed in terms of the corresponding spin wave variables $\tilde{q}_k$, $\tilde{p}_k$. Retaining up to quadratic terms in the expansion (i.e., neglecting collisions among spin waves), one finds the evolution equations

$$\begin{cases} \dfrac{d\theta}{dt} = 4[\tilde{J}_0(1-\epsilon(t)) - \delta^{pp}(t)]\sin\theta\cos\phi\sin\phi \\ \qquad\qquad + 4\,\delta^{qp}(t)\,\cos\theta\sin\theta\cos^2\phi, \\ \dfrac{d\phi}{dt} = -2B(t) + 4[\tilde{J}_0(1-\epsilon(t)) - \delta^{qq}(t)]\cos\theta\cos^2\phi \\ \qquad\qquad + 4\,\delta^{qp}(t)\,\sin\phi\cos\phi, \end{cases} \tag{C1}$$

where $\delta^{\alpha\beta}(t) \equiv 2\sum_{k\neq 0}\tilde{J}_k\Delta_k^{\alpha\beta}/N$ with $\alpha,\beta \in \{p,q\}$ is the quantum "feedback" in terms of correlation functions of the spin waves, $\Delta_k^{qq}(t) = \langle\tilde{q}_k(t)\tilde{q}_{-k}(t)\rangle$ and analogously Δ_k^{qp}, Δ_k^{pp}. The evolution of $\Delta_k^{\alpha\beta}$ is ruled by a system of differential equations involving $\theta(t)$ and $\phi(t)$ [32,33]. The validity of the quadratic approximation is controlled by the density of spin waves, $\epsilon(t) \equiv \sum_{k\neq 0}(\Delta_k^{qq} + \Delta_k^{pp} - 1)/N$ (with abuse of notation, here and in the main text we omit the brackets in denoting the quantum expectation values $\langle\vec{S}(t)\rangle$ and $\langle\epsilon(t)\rangle$). The length of the collective spin $|\vec{S}(t)| = 1 - \epsilon(t)$ is conserved by the dynamics only when $\alpha = 0$. The approximation is justified as long as the density of excited spin waves is low, i.e., $\epsilon(t) \ll 1$. Initially fully polarized, spin-coherent states, as considered in Fig. 5, correspond to the initial data for Eqs. (C1) $\theta(0) = \theta_0$, $\phi(0) = \phi_0$ with $\Delta_k^{qq}(0) = \Delta_k^{pp}(0) = 1/2$, and $\Delta_k^{qp}(0) = 0$. In particular, $\epsilon(0) = 0$.

APPENDIX D: COEXISTENCE OF KAPITZA AND FERROMAGNETIC PHASES

We briefly discuss here the coexistence of a second dynamically stabilized phase K and the ferromagnetic phases $F_{\parallel,\perp}$ in the periodically driven infinite-range Ising model (cf. Fig. 1), and the instability of the former for $\alpha \neq 0$.

For $B_0 < \tilde{J}_0(1 - |\gamma(\zeta)|)$ (i.e., within the shaded region in Fig. 1), the effective Hamiltonian Eq. (3) has a *maximum* at the paramagnetic point in addition to the two ferromagnetic minima in the xz or yz plane, depending on γ being positive or negative, respectively. The corresponding phase portraits are shown in Fig. 7. Stable trajectories exist around the direction of both the ferromagnetic minima and the paramagnetic configuration, which would be unstable in the absence of driving.

Even though dynamical stabilization of the paramagnetic configurations occurs for the collective $k = 0$ mode within this region of the parameters, a subset of the remaining modes with finite wavevectors $k \neq 0$ turn out to be unstable when $\alpha > 0$. In fact, within a linear stability analysis, the effective

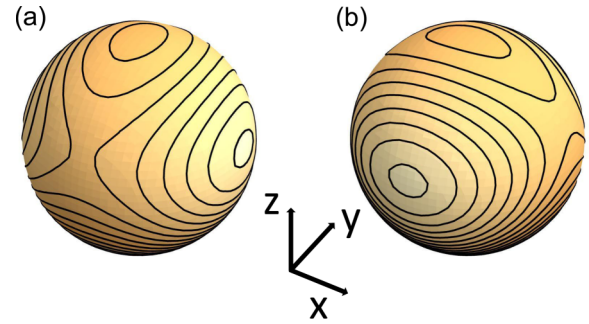

FIG. 7. Schematic phase portraits of the effective Hamiltonian $\mathcal{H}_{\text{eff}}$ in Eq. (3) on the sphere, with parameters belonging to the shaded region of the nonequilibrium phase diagram in Fig. 1, corresponding to the coexistence of a dynamically stabilized Kapitza phase and the ferromagnetic phase $F_{\parallel}$ [(a), shaded blue in Fig. 1], or $F_{\perp}$ [(b), shaded orange in Fig. 1]. We emphasize that the paramagnetic configuration is here associated with a *maximum* of $\mathcal{H}_{\text{eff}}$.

spectrum of excitations is given by

$$\omega_k^2 = 4[B_0 - (1-\gamma(\zeta))\tilde{J}_k][B_0 - (1+\gamma(\zeta))\tilde{J}_k], \tag{D1}$$

as obtained by expanding Eq. (6) in spin wave operators around $\theta = 0$, and it features an interval of k in the Brillouin zone with imaginary frequencies within the range of parameter values $B_0 < \tilde{J}_0(1 - |\gamma(\zeta)|)$ under consideration, see Fig. 8. The amplitude of this interval shrinks to zero when the anisotropy $\gamma = \mathcal{J}_0(4\zeta)$ approaches 0, i.e., when the driving strength ζ equals one of the zeros ζ_n with $n = 1, 2, \ldots$ of the Bessel function. Away from this discrete set of values, the

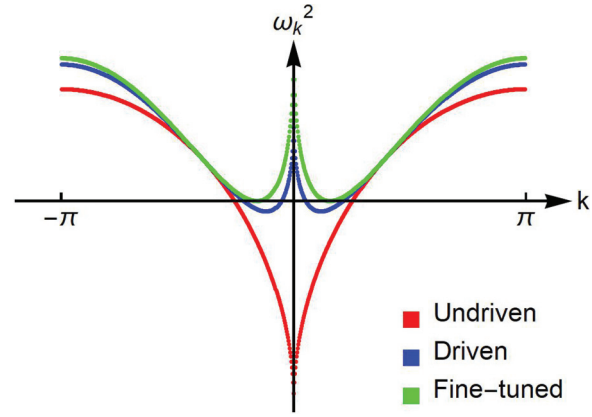

FIG. 8. Effective spectrum of the quantum spin-wave excitations around the unstable paramagnetic configuration for $\alpha = 1.5$, $N = 400$, $B_0/\tilde{J}_0 = 0.35$, in the presence of a high-frequency drive with $\delta B/\Omega = 0$ (red), 0.4023 (blue), and 0.6014 (green), corresponding to effective anisotropy parameters $\gamma = 1$, 0.45, and 0, respectively. The blue and green points correspond to parameters within the shaded region in Fig. 1, in which coexistence of Kapitza and ferromagnetic phases occurs in the infinite-range model. Although the collective $k = 0$ mode is dynamically stabilized, for $\alpha \neq 0$ an extended interval in the Brillouin zone appears with modes characterized by imaginary frequencies $\omega_k^2 < 0$, as shown, e.g., by the blue points. This instability disappears only at isotropic points $\zeta_1, \zeta_2, \ldots$ for which $\gamma = 0$ [corresponding to the zeros of the Bessel function, see after Eq. (3)], as shown by the green points.

Kapitza phase coexisting with the ferromagnetic phases turns out to be destabilized by these finite-wavelength fluctuations, at least at the level of linear stability, although the collective $k = 0$ mode is dynamically stabilized.

It is interesting to note that when ζ is tuned to an isotropic point ζ_n, the many-body Kapitza phase discussed above becomes stable in the high-frequency limit $\Omega \to \infty$, and thus approximately stable for $\Omega \gg \tilde{J}_0$. The reason behind such stability can be easily traced back to the stroboscopic conservation of S_z: Indeed, if the system is initialized in a fully polarized state with a small displacement θ_0 from the z axis, the collective spin has to remain trapped in a neighborhood of the otherwise unstable configuration $\theta = 0$, because $S_z(t_n = nT) \approx 1 - \theta_0^2/2$ cannot decrease.

APPENDIX E: NONEQUILIBRIUM PHASE DIAGRAM FOR $\alpha > 0$

Here we discuss the modification of the phase boundaries in Fig. 1 when α increases from 0 to 2 and beyond, leading to Fig. 4. These boundaries are determined by the critical value $B_0 = B_{\rm cr}(\zeta)$ below which the high-frequency effective Hamiltonian Eq. (6) develops ferromagnetic ordering, either in the xz or in the yz plane depending on the anisotropy $\gamma(\zeta)$ being positive or negative, respectively. Ferromagnetic ordering arises as soon as tilted spin configurations, with average orientation forming an angle $\theta \neq 0$ with the field direction z, acquire a lower energy than the paramagnetic states with $\theta = 0$.

In the infinite-range case $\alpha = 0$, the critical line is determined by $B_{\rm cr}(\zeta) = \tilde{J}_0(1 + |\gamma(\zeta)|)$, in correspondence of which the energy landscape $\mathcal{E}_{\rm eff}(\theta) \equiv \langle H_{\rm eff}\rangle_{\theta,\phi^*}$ [with $\phi^* = 0$ or $\pi/2$ depending on $\gamma(\zeta) > 0$ or <0, respectively] of the semiclassical collective spin $\vec{S} = (\sin\theta\cos\phi, \sin\theta\sin\phi, \cos\theta)$ changes from a single well for $B_0 > B_{\rm cr}(\zeta)$, with the minimum at $\theta^* = 0$, to a symmetric double well for $B_0 < B_{\rm cr}(\zeta)$, with the minima at $\theta^* = \pm\arccos(B_0/B_{\rm cr}(\zeta))$.

In the presence of an interaction with $\alpha \neq 0$, the quantum fluctuations of all the spin degrees of freedom with Fourier wave vector $k \neq 0$ modify the effective energy landscape $\mathcal{E}_{\rm eff}(\theta)$ of the collective spin, thereby shifting the critical value of B_0 to $B_{\rm cr}(\zeta) \equiv \tilde{J}_0(1 + |\gamma(\zeta)|) + \Delta B_{\rm cr}(\zeta)$. Within the spin-wave treatment introduced in Refs. [32,33], we can compute $\mathcal{E}_{\rm eff}(\theta)$ and hence the shift $\Delta B_{\rm cr}(\zeta)$ to lowest order in $\tilde{J}_{k\neq 0}$, via a variational approach. In particular, we consider the expansion of $H_{\rm eff}$ to quadratic order in the spin-wave operators around the direction in the xz or yz plane identified by the angle θ, resulting in Eq. (4) with $\phi = 0$ or $\pi/2$, respectively, and we determine the energy landscape $\mathcal{E}_{\rm eff}(\theta) \equiv \min_\psi \langle H_{\rm eff}\rangle_\psi$ by computing the parametric spin-wave ground-state energy. We obtain

$$\frac{\mathcal{E}_{\rm eff}(\theta)}{N} = -\tilde{J}_0\frac{1+|\gamma|}{2}\sin^2\theta - B_0\cos\theta + \frac{1}{N/2}\sum_{k\neq 0}\frac{\omega_k - \omega_k^{(0)}}{2}, \tag{E1}$$

where

$$\omega_k^2 = 4[\tilde{J}_0(1+|\gamma|)\sin^2\theta - \tilde{J}_k(1+|\gamma|)\cos^2\theta + B_0\cos\theta] \times [\tilde{J}_0(1+|\gamma|)\sin^2\theta - \tilde{J}_k(1-|\gamma|) + B_0\cos\theta] \tag{E2}$$

and

$$\omega_k^{(0)} = 2[\tilde{J}_0(1+|\gamma|)\sin^2\theta + B_0\cos\theta] = \omega_k|_{\tilde{J}_{k\neq 0}=0}. \tag{E3}$$

The last term in Eq. (E1) represents the zero-point contribution of quantum fluctuations with arbitrary k. The energy landscape $\mathcal{E}_{\rm eff}(\theta)$ in Eq. (E1) can be expanded at small θ as

$$\mathcal{E}_{\rm eff}(\theta) = \mathcal{E}_{\rm eff}(\theta = 0) + \omega_{\rm eff}(B_0)\frac{\theta^2}{2} + \mathcal{O}(\theta^4), \tag{E4}$$

and the critical value $B_{\rm cr}$ of B_0 is determined by the equation $\omega_{\rm eff}(B_0) = 0$, corresponding to the transition from a single ($\omega_{\rm eff} > 0$) to a double ($\omega_{\rm eff} < 0$) well landscape. The solution may be found by formally expanding B_0 in powers of $\tilde{J}_{k\neq 0}$ and equating both sides order by order. This procedure yields

$$B_{\rm cr}(\zeta) = \tilde{J}_0\big(1+|\gamma(\zeta)|\big) \times\left\{1 - \frac{2|\gamma(\zeta)| + 3|\gamma(\zeta)|^2}{4\big(1+|\gamma(\zeta)|\big)^2}\left[\int_{-\pi}^{\pi}\frac{dk}{\pi}\left(\frac{\tilde{J}_k}{\tilde{J}_0}\right)^2\right]\right\} + \mathcal{O}\big(\tilde{J}_k^3\big), \tag{E5}$$

which yields the negative quadratic correction $\Delta B_{\rm cr}$ reported in Eq. (7). This implies that the quantum fluctuations destabilize the ferromagnetic ordering, as expected on physical grounds. Moreover, we observe that the shift $\Delta B_{\rm cr}$ of the critical value is maximal for $\gamma = 1$ and vanishes at isotropic points with $\gamma = 0$, as illustrated in Fig. 4. Note that this result is valid for any type of spatial dependence $J_{|i-j|}$ of the interactions in Eq. (1).

We finally remark that in the opposite limit $\alpha = \infty$, the system Eq. (1) reduces to the standard quantum Ising chain with nearest-neighbor interactions (which has been studied in Refs. [39,47]). In this case, the effective high-frequency Hamiltonian Eq. (6) describes the XY quantum spin chain, which is exactly solvable in terms of free fermions [48]. Correspondingly, the quantum critical point $B_{\rm cr} = \tilde{J}_0$ is independent of γ, and thus of the driving strength ζ. Accordingly, it is natural to conjecture that the left boundary of the Kapitza phase in Fig. 4 moves leftwards as α exceeds 1, and eventually approaches the straight vertical line $B_{\rm cr}(\zeta) = \tilde{J}_0$ when $\alpha \to \infty$. However, it is important to note that ferromagnetic ordering cannot arise at finite energy density for $\alpha > 2$. Thus, in this case the equilibrium phase diagram of the effective Hamiltonian does not straightforwardly provide information on the dynamics in the presence of the driving.

[1] M. Grifoni and P. Hänggi, Driven quantum tunneling, Phys. Rep. **304**, 229 (1998).

[2] M. Bukov, L. D'Alessio, and A. Polkovnikov, Universal high-frequency behavior of periodically driven systems: From dynamical stabilization to Floquet engineering, Adv. Phys. **64**, 139 (2015).

[3] M. Holthaus, Floquet engineering with quasi-energy bands of periodically driven optical lattices, J. Phys. B: At. Mol. Opt. Phys. **49**, 013001 (2016); A. Eckhardt, Colloquium: Atomic quantum gases in periodically driven optical lattices, Rev. Mod. Phys. **89**, 011004 (2017).

[4] N. Goldman and J. Dalibard, Periodically Driven Quantum Systems: Effective Hamiltonians and Engineered Gauge Fields, Phys. Rev. X **4**, 031027 (2014); M. Heyl, P. Hauke, and P. Zoller, Quantum localization bounds Trotter errors in digital quantum simulation, Sci. Adv. **5**, eaau8342 (2019).

[5] T. Kitagawa, E. Berg, M. Rudner, and E. Demler, Topological characterization of periodically-driven quantum systems, Phys. Rev. B **82**, 235114 (2010); N. Lindner, G. Refael, and V. Galitski, Floquet topological insulator in semiconductor quantum wells, Nat. Phys. **7**, 490 (2011).

[6] F. Wilczek, Superfluidity and Space-Time Translation Symmetry Breaking, Phys. Rev. Lett. **111**, 250402 (2013); H. Watanabe and M. Oshikawa, Absence of Quantum Time Crystals, *ibid.* **114**, 251603 (2015); N. Y. Yao, A. C. Potter, I.-D. Potirniche, and A. Vishwanath, Discrete Time Crystals: Rigidity, Criticality, and Realizations, *ibid.* **118**, 030401 (2017).

[7] J. Zhang, P. W. Hess, A. Kyprianidis, P. Becker, A. Lee, J. Smith, G. Pagano, I.-D. Potirniche, A. C. Potter, A. Vishwanath, N. Y. Yao, and C. Monroe, Observation of a discrete time crystal, Nature (London) **543**, 217 (2017); S. Choi *et al.*, Observation of discrete time crystalline order in a disordered dipolar many-body system, *ibid.* **543**, 221 (2017).

[8] D. H. Dunlap and V. M. Kenkre, Dynamical localization of a charged particle moving under the influence of an electric field, Phys. Rev. B **34**, 3625 (1986); Effect of scattering on the dynamic localization of a particle in a time-depedent electric field, **37**, 6622 (1988); A. Eckardt, C. Weiss, and M. Holthaus, Superfluid-Insulator Transition in a Periodically Driven Optical Lattice, Phys. Rev. Lett. **95**, 260404 (2005); A. Zenesini, H. Lignier, D. Ciampini, O. Morsch, and E. Arimondo, Coherent Control of Dressed Matter Waves, *ibid.* **102**, 100403 (2009).

[9] P. L. Kapitza, Dynamic stability of a pendulum when its point of suspension vibrates, Soviet Phys. JETP **21**, 588 (1951).

[10] E. D. Courant, M. S. Livingston, and H. S. Snyder, The strong-focusing synchroton—A new high energy accelerator, Phys. Rev. **88**, 1190 (1952).

[11] G. Zs. K. Horvath, R. C. Thompson, and P. L. Knight, Fundamental physics with trapped ions, Contemporary Phys. **38**, 25 (1997).

[12] H. Saito and M. Ueda, Dynamically Stabilized Bright Solitons in a Two-Dimensional Bose-Einstein Condensate, Phys. Rev. Lett. **90**, 040403 (2003); F. K. Abdullaev, J. G. Caputo, R. A. Kraenkel, and B. A. Malomed, Controlling collapse in Bose-Einstein condensates by temporal modulation of the scattering length, Phys. Rev. A **67**, 013605 (2003).

[13] W. Zhang, B. Sun, M. S. Chapman, and L. You, Localization of spin mixing dynamics in a spin-1 Bose-Einstein condensate, Phys. Rev. A **81**, 033602 (2010).

[14] T. M. Hoang, C. S. Gerving, B. J. Land, M. Anquez, C. D. Hamley, and M. S. Chapman, Dynamic Stabilization of a Quantum Many-Body Spin System, Phys. Rev. Lett. **111**, 090403 (2013).

[15] F. K. Abdullaev and R. A. Kraenkel, Macroscopic quantum tunneling and resonances in coupled Bose-Einstein condensates with oscillating atomic scattering length, Phys. Lett. A **272**, 395 (2000); E. Boukobza, M. G. Moore, D. Cohen, and A. Vardi, Nonlinear Phase Dynamics in a Driven Bosonic Josephson Junction, Phys. Rev. Lett. **104**, 240402 (2010).

[16] M. Kac and C. J. Thompson, Critical behavior of several lattice models with long-range interaction, J. Math. Phys. **10**, 1373 (1969); A. Campa, T. Dauxois, D. Fanelli, and S. Ruffo, *Physics of Long-Range Interacting Systems* (Oxford University Press, Oxford, 2015).

[17] J. Zhang *et al.*, Observation of a many-body dynamical phase transition with a 53-qubit quantum simulator, Nature (London) **551**, 601 (2017).

[18] R. Blatt and C. F. Roos, Quantum simulations with trapped ions, Nat. Phys. **8**, 277 (2012).

[19] H. Bernien, S. Schwartz, A. Keesling, H. Levine, A. Omran, H. Pichler, S. Choi, A. S. Zibrov, M. Endres, M. Greiner, V. Vuletić, and M. D. Lukin, Probing many-body dynamics on a 51-atom quantum simulator, Nature (London) **551**, 579 (2017).

[20] H. Labuhn, D. Barredo, S. Ravets, S. de Léséleuc, T. Macrì, T. Lahaye, and A. Browaeys, Tunable two-dimensional arrays of single Rydberg atoms for realizing quantum Ising models, Nature (London) **534**, 667 (2016); S. de Léséleuc, S. Weber, V. Lienhard, D. Barredo, H. Peter Büchler, T. Lahaye, and A. Browaeys, Accurate Mapping of Multilevel Rydberg Atoms on Interacting Spin-1/2 Particles for the Quantum Simulation of Ising Models, Phys. Rev. Lett. **120**, 113602 (2018).

[21] H. Lipkin, N. Meshkov, and A. Glick, Validity of many-body approximation methods for a solvable model: (I) Exact solutions and perturbation theory, Nucl. Phys. **62**, 188 (1965).

[22] B. Sciolla and G. Biroli, Dynamical transitions and quantum quenches in mean-field models, J. Stat. Mech. (2011) P11003.

[23] B. Žunkovič, A. Silva, and M. Fabrizio, Dynamical phase transitions and Loschmidt echo in the infinite-range XY model, Phil. Trans. R. Soc. A **374**, 20150160 (2016).

[24] G. Engelhardt, V. M. Bastidas, C. Emary, and T. Brandes, ac-driven quantum phase transition in the Lipkin-Meshkov-Glick model, Phis. Rev. E **87**, 052110 (2013).

[25] A. Das, K. Sengupta, D. Sen, and B. Chakrabarti, Infinite-range Ising ferromagnet in a time-dependent transverse magnetic field: Quench and ac dynamics near the quantum critical point, Phys. Rev. B **74**, 144423 (2006).

[26] A. Russomanno, R. Fazio, and G. Santoro, Thermalization in a periodically driven fully-connected quantum Ising ferromagnet, Europhys. Lett. **110**, 37005 (2015).

[27] M. C. Gutzwiller, *Chaos in Classical and Quantum Mechanics*, Interdisciplinary Applied Mathematics (Springer-Verlag, New York, 1990).

[28] J. Pöschel, A lecture on the classical KAM theorem, Proc. Symp. Pure Math. **69**, 707 (2001).

[29] J. Tomkovič, W. Muessel, H. Strobel, S. Löck, P. Schlagheck, R. Ketzmerick, and M. K. Oberthaler, Experimental observation of the Poincaré-Birkhoff scenario in a driven many-body quantum system, Phys. Rev. A **95**, 011602(R) (2017).

[30] L. D. Landau and E. M. Lifshitz, *Mechanics*, Course of Theoretical Physics S (Butterworth-Heinemann, 1976); H. W. Broer, I. Hoveijn, M. van Noort, C. Simó, and G. Vegter, J. Dyn. Diff. Equat. **16**, 897 (2004).

[31] S. Blanes, F. Casas, J. A. Orteo, and J. Ros, The Magnus expansion and some of its applications, Phys. Rep. **470**, 151 (2009).

[32] A. Lerose, J. Marino, B. Žunkovič, A. Gambassi, and A. Silva, Chaotic Dynamical Ferromagnetic Phase Induced by Non-Equilibrium Quantum Fluctuations, Phys. Rev. Lett. **120**, 130603 (2018).

[33] A. Lerose, B. Žunkovič, J. Marino, A. Gambassi, and A. Silva, Impact of non-equilibrium fluctuations on pre-thermal dynamical phase transitions in interacting spin chains, Phys. Rev. B **99**, 045128 (2019).

[34] C. Itzykson and J.-M. Drouffe, *Statistical Field Theory*, Vol. 312 (WILEY-VCH Verlag GmbH & Co., New York, 1991), p. 412.

[35] L. D'Alessio and M. Rigol, Long-time behavior of isolated periodically driven interacting lattice systems, Phys. Rev. X **4**, 041048 (2014).

[36] D. Abanin, W. De Roeck, and F. Huveneers, Exponentially Slow Heating in Periodically Driven Many-Body Systems, Phys. Rev. Lett. **115**, 256803 (2015); D. Abanin, W. De Roeck, W. W. Ho, and F. Huveneers, Effective Hamiltonians, prethermalization, and slow energy absorption in periodically driven many-body systems, Phys. Rev. B **95**, 014112 (2017); T. Mori, T. Kuwahara, and K. Saito, Rigorous Bound on Energy Absorption and Generic Relaxation in Periodically Driven Quantum Systems, Phys. Rev. Lett. **116**, 120401 (2016); F. Machado, G. D. Meyer, D. V. Else, C. Nayak, and N. Y. Yao, Exponentially slow heating in short and long-range interacting Floquet systems, arXiv:1708.01620

[37] S. Weidinger and M. Knap, Floquet prethermalization and regimes of heating in a periodically driven, interacting quantum system, Sci. Rep. **7**, 45382 (2017).

[38] T. Shirai, J. Thingna, T. Mori, S. Denisov, P. Hänggi, and S. Miyashita, Effective Floquet-Gibbs states for dissipative quantum systems, New J. Phys. **18**, 053008 (2016).

[39] A. Russomanno, A. Silva, and G. E. Santoro, Periodic Steady Regime and Interference in a Periodically Driven Quantum System, Phys. Rev. Lett. **109**, 257201 (2012).

[40] A. Lazarides, A. Das, and R. Moessner, Periodic Thermodynamics of Isolated Quantum Systems, Phys. Rev. Lett. **112**, 150401 (2014).

[41] E. Canovi, M. Kollar, and M. Eckstein, Stroboscopic prethermalization in weakly interacting periodically driven systems, Phys. Rev. E **93**, 012130 (2016).

[42] M. Bukov, S. Gopalakrishnan, M. Knap, and E. Demler, Prethermal Floquet Steady States and Instabilities in the Periodically Driven, Weakly Interacting Bose-Hubbard Model, Phys. Rev. Lett. **115**, 205301 (2015).

[43] R. Citro, E. G. Dalla Torre, L. D'Alessio, A. Polkovnikov, M. Babadi, T. Oka, E. Demler, Dynamical stability of a many-body Kapitza pendulum, Ann. Phys. **360**, 694 (2015).

[44] L. D'Alessio and A. Polkovnikov, Many-body energy localization transition in periodically driven systems, Ann. Phys. **333**, 19 (2013).

[45] J. W. Britton, B. C. Sawyer, A. C. Keith, C.-C. Joseph Wang, J. K. Freericks, H. Uys, M. J. Biercuk, and J. J. Bollinger, Engineered two-dimensional Ising interactions in a trapped-ion quantum simulator with hundreds of spins, Nature (London) **484**, 489 (2012).

[46] C. Senko, P. Richerme, J. Smith, A. Lee, I. Cohen, A. Retzker, and C. Monroe, Realization of a Quantum Integer-Spin Chain with Controllable Interactions, Phys. Rev. X **5**, 021026 (2015).

[47] V. M. Bastidas, C. Emary, G. Schaller, and T. Brandes, Nonequilibrium quantum phase transitions in the Ising model, Phys. Rev. A **86**, 063627 (2012); M. Benito, A. Gomez-Leon, V. M. Bastidas, T. Brandes, and G. Platero, Floquet eingineering of long-range *p*-wave superconductivity, Phys. Rev. B **90**, 205127 (2014).

[48] E. Lieb, T. Schultz, and D. Mattis, Two soluble models of an antiferromagnetic chain, Ann. Phys. **16**, 407 (1961).